Spatial Resolution Limits for Synchrotron-based Spectromicroscopy in the Mid- and Near-Infrared

Erika Levenson[1], Philippe Lerch[2], and Michael C. Martin[1*]

[1]Advanced Light Source Division, Lawrence Berkeley National Laboratory,
1 Cyclotron Road, Berkeley, CA 94720, USA
[2]Swiss Light Source, Paul Scherrer Institut, 5232 Villigen, Switzerland

Synopsis

Spatial resolution measurements at ALS Beamline 1.4.4 are used to determine the wavelengths at which a cross-over from diffraction-limited to electron beam source size-limited resolution occurs. Performance is then predicted for different synchrotrons, beamline optics, and endstation microscopes.

Abstract

Spatial resolution tests were performed on beamline 1.4.4 at the Advanced Light Source in Berkeley, CA, a third generation synchrotron light source. This beamline couples the high-brightness synchrotron source to a Thermo-Electron Continuμm XL infrared microscope. Two types of resolution tests were performed in both the mid-IR and near-IR. The results are compared to a diffraction-limited spot size theory. At shorter near-IR wavelengths the experimental results begin to deviate diffraction-limited so a combined diffraction-limit and electron-beam source size model is employed. This description shows how the physical electron beam size of the synchrotron source begins to dominate the focused spot size at higher energies. The transition from diffraction-limited to electron beam size-limited performance is a function of storage ring parameters and the optical demagnification within the beamline and microscope optics. The discussion includes how different facilities, beamlines, and microscopes will affect the acheivable spatial resolution. As synchrotron light sources and other next generation accelerators such as energy recovery LINAC's and free-electron lasers achieve smaller beam emittances, beta-functions, and/or energy spreads, diffraction-limited performance can continue to higher energy beams, perhaps ultimately into the extreme ultraviolet.

Keywords: Infrared, Resolution, Microscopy, FTIR, Spectromicroscopy, Imaging, Diffraction, Emittance, Microspectroscopy, Beamline

[*] Author to whom correspondence should be addressed: 510-495-2231, MCMartin@lbl.gov

Introduction

Synchrotron infrared beamlines provide diffraction-limited spatial resolution for spectromicroscopy with high signal to noise (Reffner *et al.*, 1995; Carr *et al.*, 1995; Carr, 2001; Martin & McKinney 1998; Martin & McKinney 2001). The synchrotron has 100 – 1000 times higher brightness than a conventional thermal globar source (Reffner *et al.*, 1995; Carr *et al.*, 1995; Martin & McKinney, 2001; Holman *et al.*, 2003, Dumas & Tobin, 2003; Holman & Martin, 2006) enabling a wide variety of new science at small spatial scales (Holman et al., 2000; Raab & Martin, 2001; Holman *et al.*, 2003; Dumas & Tobin, 2003; Miller *et al.*, 2003, Bertrand *et al.*, 2003; Holman & Martin, 2006; Miller & Dumas, 2006; Li *et al.*, 2006; Keller *et al.,* 2006; Veiseh *et al.,* 2007). We have previously verified the diffraction-limited performance through the mid-IR of the infrared beamlines at the Advanced Light Source (ALS), in Berkeley (Levenson *et al.*, 2006). However as the synchrotron emission wavelength becomes shorter and shorter, the physical size of the electron beam will become the dominant factor for the photon source size.

The source size of a synchrotron light beam can be approximated well by adding in quadrature the effects of diffraction, the electron beam size, and the projected size of the emitting region (Hirschmugl, 1994, Reffner *et al.*, 1995; Carr *et al.*, 1995; Carr, 2001;). This source is then imaged to a focused spot on a sample via beamline optics that have an overall demagnification factor, *m*. In practice we have found that after all the beamline collection, collimation and refocussing optics, the effects of diffraction and electron beam size dominate over the projected size of the emitting region, so for this analysis we neglect the latter. The spot size can therefore be written as

$$m\sqrt{(d_R\lambda)^2 + \sigma_t^2} \tag{1}$$

where d_R is a diffraction limit factor (depends on which resolution model is chosen, as described later), λ is the wavelength of light, and σ_t is the transverse synchrotron electron beam size. As both the electron and photon beams are usually measured and approximated as Gaussian in profile, one must use consistent Gaussian line-width definitions (such as σ or full width half max, FWHM) in applying Eqn. 1. In a synchrotron, the transverse electron beam size is given by

$$\sigma_t = \sqrt{\beta_t \varepsilon_t + \eta_t^2 \left(\frac{\sigma_E}{E} \right)^2} \tag{2}$$

where β_t is the beta-function, ε_t is the emittance, η_t is the dispersion (all in the transverse to the electron beam's direction, t can be x or y), and σ_E/E is the energy spread (Kim, 1989). These parameters are specific to each storage ring, its operating conditions, and the specific location within the magnetic lattice that the light is being emitted from. These parameters and thus the electron beam sizes in the x and y directions for any specific synchrotron beamline are well known for normal storage ring operations and typically can be found in the machine data sections of individual light source web sites.

Experiment

We performed lateral resolution testing experiments as a function of wavelength in the mid- and near-IR at ALS beamline 1.4.4. A Thermo-Electron Continuμm XL microscope is installed on on this beamline along with a Thermo-Electron Nexus 870 FTIR bench which has been modified with an offset laser scanner (similar to the newer Nexus 8700 model). The light from the synchrotron is collected from the 1.4 port using 10 mrad vertical by 40 mrad horizontal collection optics. The front end optics refocus with a 1:1 image at a diamond window which lets the light beam exit the ultra-high vacuum. A pair of cylindrical mirrors are used to collimate the x and y directions of this source before steering the light into the emission port of the FTIR bench. The light is modulated and then passed through the IR microscope and is focused onto the sample using all reflective 15× or 32× cassegrain objectives with numerical apertures (N.A.) of 0.58 and 0.65 respectively. The results presented here were obtained with the 32× objective, however very similar results were also obtained with the 15× objective. The sample stage is a Prior Scientific H101 stage which is computer controlled with step sizes as small as 0.1 microns. All measurements were done in reflection mode without any apertures in the light path, and the results presented here detail the y-direction cross-sections of the focused spot[†].

[†] We chose the y-direction because the x-direction does not fill the full N.A. of the objective in the reflection mode in this microscope. This (and possibly other beamline optical effects) causes the y-direction to have an experimentally measured better focus than the x-direction, so the y-direction should be closer to diffraction-limited with the N.A. stated for the objective.

We previously published mid-IR resolution test results showing the resolution is indeed diffraction-limited (Levenson *et al.*, 2006), so for this study we concentrate on the near-IR. An MCT-A* detector was used for wavenumbers ranging form 2000 cm^{-1} to 7000 cm^{-1}. The MCT-A* was swapped with the InGaAs detector to study wavenumbers from 5000 cm^{-1} to 11000 cm^{-1}. A CaF_2 beamsplitter was used to cover this entire range.

Spatial resolution tests were performed using a high-resolution USAF 1951 3-Bar Resolving Test Chart (MIL-STD-150A) from Applied Image Inc. (Rochester, NY). The USAF resolution test sample has a chrome metal coating on a glass substrate with the resolution test structures patterned in a negative image up to a frequency of 512 cycles/mm (smallest is Group 9, Element 3).

Two types of resolution tests were done. The first is a step edge (or knife edge) test. The test is performed stepping the sample from a position where the infrared beam is focused on the reflective metal coating to where the beam is focused on the absorbing glass pattern (see Figure 1(c)). A spectrum is acquired at each point and a profile of the reflectivity as a function of position and wavelength is obtained. The first derivative of the profile is calculated and fit to a Gaussian function. The full width half max (FWHM) of the Gaussian fit determines the resolution as demonstrated in Figure 1(a) (Russ, 2002).

The second type of resolution test, whose definition is shown graphically in Figure 1(b), is an imaging resolution test done by scanning across three bars of the same width and distance apart. Once a reflectance profile is obtained via a line map across a set of three bars, Rayleigh's criterion (Rayleigh, 1879; Hecht, 1998; Born & Wolf, 1999) is used to determine whether the bars are resolved or not. As shown in Fig. 1(b), Rayleigh's criterion states that if the minimum intensity between two peaks (I) is less than $8/\pi^2$ the intensity of the peaks (I_o), then the bars are resolved.

These two definitions are well known from the literature, however it is important to note that they yield different numerical results since they are based on different definitions. The Rayleigh

imaging criterion will give a higher resolution than the FWHM step-edge analysis by a factor of $1/2$ (half maximum) to $8/\pi^2$, which is 0.617.

Analyses were completed for wavelengths from 1.11 μm to 6.5 μm for the imaging resolution tests and between 0.91 μm to 5 μm for the step edge resolution tests.

Step Edge Resolution Test Results

The MCT-A* detector was used for wavelengths from 1.43-5 μm and the InGaAs detector and the CaF2 beamsplitter were used for wavelengths from 0.91-2 μm. The step edge tests were performed using the 32× objective. Example measured profiles for each analyzed wavelength are shown in the inset to Figure 2. The derivative of each line profile was fit to a Gaussian and Figure 2 plots FWHM resolution versus wavelength for both detectors. A simple linear fit to the data is reasonable and yields a resolution for the synchrotron source of (0.73 ± 0.04) λ.

This, however, does not follow the theoretical diffraction limit as the intercept of this linear fit does not pass through the origin, therefore it underestimates the slope of the real data, plus the fit becomes worse at shorter wavelengths. An improved and more physically meaningful fit is obtained by using equation (1) which includes the effects of diffraction and the physical size of the electron beam. In this case the best fit results in the diffraction portion of the data is given by (0.81 ± 0.02) λ, with a demagnified electron beam size of 0.71 ± 0.11 μm. Demagnification shall be discussed further in the paper.

Imaging Resolution Test Results

Imaging tests were done with the synchrotron source with both objectives. Analyses based on Rayleigh's criterion were completed at wavelengths between 6.5 and 1.11 μm. The inset in Figure 3 shows Gaussian fits to the profiles of the smallest bars for 7000 cm^{-1} (λ = 1.43 μm) and 9000 cm^{-1} (λ = 1.11 μm). Only the 9000 cm^{-1} profile meets Rayleigh's criterion of being resolved. The measured resolutions of all wavelengths analyzed are presented in Figure 3. A simple linear fit to the data yields a resolution of (0.45 ± 0.02) λ.

Again, however, this simple linear fit does not adequately follow the data point particularly at shorter wavelengths, nor does it intercept the origin. The experimental imaging data more clearly shows the deviation from a simple diffraction-limited spot size at short wavelengths. An improved fit is found using Equation (1) with the diffraction portion of the data given by (0.47 ± 0.01) λ, and a demagnified electron beam size of 0.51 ± 0.06 μm.

Analysis

As noted above, the step-edge and imaging tests use different resolution definitions and the results should be different by a factor of 0.617. Indeed we find that the diffraction portion of the best fits to Eqn. 1 are different by a factor of 0.59 ± 0.03 and the electron beam size portions of the fits are different by a factor of 0.72 ± 0.20. Both differences match the ideal difference factor of 0.617 within the error bars and so we conclude that the two resolution tests give consistent results.

The electron beam source size for the 1.4 (22.6 degree) bending magnet port at the ALS is σ_x = 65 μm and σ_y = 52 μm (ALS Storage Ring Parameters). These are one sigma values, and the FWHM beam size is 2.35 times larger (Russ, 1986). Thus, the electron beam size is 153 μm in the horizontal and 122 μm in the vertical dimension.

The magnification factor *m* for the 1.4 beamline is given by the ratio of the focal distance of the collimating mirror to the focal distance of the microscope objective focusing the light onto the sample. We use a 300 mm radius (150 mm focal distance) cylindrical mirror to collimate the 40 mrad horizontal to a 6 mm beam size. In the vertical, we collimate the 10 mrad beam with a 1200 mm radius (600 mm focal distance) cylinder to again achieve a 6 mm beam size. This 6 × 6 mm beam is modulated by the FTIR interferometer, passes through the infrared microscope to the cassegrain objective which focuses the light onto the sample. The cassegrain expands the beam with the secondary mirror, followed by focusing with the larger primary mirror. For simplicity instead of following the complexities of the cassegrain, we can mentally substitute the cassegrain for a simple thin lens, whose focal length is the distance it takes to focus a 6 mm beam to a point using the cassegrain's correct N.A. value. Thus the effective focal distance to the sample (the distance from the sample at which the input beam is 6 mm in size based on the

N.A. of the objective – which would be the focal length of this substitute thin lens) is 3.5 mm for the 32×, and 4 mm for the 15× objective based on their N.A.'s of 0.65 and 0.58, respectively.

The beamline 1.4.4 optics image the vertical synchrotron emission to the y-direction on the sample stage which is the direction in which the spot size measurements are detailed above. The magnification factor for the 32× objective is therefore m = 171, and thus we would predict that the FWHM electron beam size of 122 μm is imaged onto the sample stage to 0.71 μm, FWHM. Or using the Rayleigh criterion, the imaged beam size is 0.44 μm. These values are in good agreement with experimental data of the demagnified electron beam source size fits of 0.71 ± 0.11 μm, and 0.51 ± 0.06 μm, for the two resolution definitions, respectively.

The usual Rayleigh criterion definition for diffraction-limited lateral resolution is two adjacent points are just resolved when the centers of their Airy disks are separated by the central Airy disk radius. For an ideal objective (and identical condenser), this limit is given by $\frac{1.22\lambda}{2NA}$. The imaging definition Rayleigh criterion we defined in Figure 1(b), however, is when the central Airy disks of adjacent point are separated by ½ of their radius, so here the Rayleigh diffraction-limited resolution is $\frac{1.22\lambda}{4NA}$. For the 32× objective with NA=0.65, we therefore expect the diffraction limited performance of this objective to be 0.47 λ. This is in excellent agreement with the fit to our measured data of (0.47 ± 0.01) λ.

Resolution performance of different synchrotron beamlines

The achievable transverse resolution of a given synchrotron beamline is a combination of the beamline optics (demagnification factor) and the electron beam source size which is dependent on the specific machine and photon port parameters. The demagnification factor achievable depends not only on the front end collection optics, but also on the final focusing objective in the IR microscope. The Thermo-Electron 15× and 32× objectives have relatively large N.A.'s, whereas the Bruker Optics 15× and 36× objectives have longer working distances but smaller N.A.'s of 0.4 and 0.5, respectively. The effective focal lengths for a 6 mm input beam for these

two objectives will be 6.9 mm and 5.2 mm, respectively, which will yield smaller magnification factors for the same front-end optics and therefore the electron-beam source demagnified on the sample stage using these objectives will be factors of 2 and 1.5 larger. This means that the effects of the electron beam source size will start at longer wavelengths and will limit the ultimate lateral spatial resolution achievable. If we were to use the Bruker 15× objective (N.A = 0.4) on the ALS IR beamline with all other optics being the same, we should obtain a spot size given by 0.76 λ for the diffraction-limit, and 0.88 μm imaged electron beam size. Other Cassegrain objectives are available from, for example, Ealing Catalog Inc. (Rocklin, CA, USA) with higher and lower magnifications (15× up to 74×) and N.A.'s (0.28 up to 0.65, respectively). Examples of the predicted resolution as a function of wavelength using different N.A. objectives are plotted in Figure 4. The choice of objective for a given beamline and/or experiment will therefore be a trade-off between higher spatial resolution and greater working distance.

The vertical electron beam source size at the ALS BL1.4 port is σ_y = 52 μm. If this beamline was placed on the smallest source size port at the ALS (x.2 or x.3 ports) the vertical electron beam size is only σ_y = 15 μm, or a factor of 3.5 smaller. This would have minimal effect to the resolution in most of the mid-IR, but the diffraction-limited performance would extend into the near-IR and a significant improvement in resolution could be achieved for wavelengths shorter than about 2 microns. If the same beamline was built at the NSLS VUV ring (a 2nd generation synchrotron which has similar IR microscopy beamlines with similar IR microscopes), the bend magnet vertical electron beam source size is σ_y = 185 μm (VUV Storage Ring Parameters, 2006), or about 3.5 times larger than the ALS 1.4 port. In this case the electron beam source size will play a more dominant role in the total effective resolution, yielding about 0.5 microns larger spot size (a 25% increase) at λ = 5 μm (2000 cm^{-1}), extending to 1 micron larger spot size (double) at λ = 2 μm (5000 cm^{-1}) compared to ALS BL1.4. An IR microscopy beamline is being built at the new SOLEIL synchrotron (France) which will use the same Continumm microscope. The planned source size for the port to be used for IR at SOLEIL is σ_y = 24.9 μm (SOLEIL Parameters at the Source points), so assuming similar magnification optics to the ALS the diffraction limited performance will continue to wavelengths shorter than 1 micron (10,000 cm^{-1}). Figure 4 presents these comparisons graphically.

The source size at the IR port currently being commissioned at the Swiss Light Source (SLS) storage ring is expected to be σ_x = 52 μm and σ_y = 26 μm. Radiation is transported with 1 to 1 optics through a diamond, Si or BaF_2 window into a mirror box which collimates the beam and steers it to the beam-splitter of a FTIR spectrometer. The magnification factor *m* at the SLS IR beamline is 86 (with a 0.58 N.A objective) and 82 (with a 0.61 N.A objective). This means that the σ_y = 26 μm vertical electron beam size will be imaged to the sample with a FWHM of 0.7 μm, or 0.43 μm using the Rayleigh definition. These values are very close to those measured at the ALS so we would predict very similar resolution capabilities assuming the use of a similar microscope objective (shown in Figure 4).

The natural vertical angle of the emitted photon beam is a function of wavelength and will decrease as the wavelength gets shorter. This will become smaller than the collected angle of a given beamline and therefore care must be taken to correctly calculate the demagnification factor *m* as the photon energy goes beyond the infrared regime. The under development NSLS-II storage ring is planned to perform at close to the theoretical minimum emittance (Kim, 1989; Summary of NSLS-II Source Properties) possible for a storage ring. The source size in the bending magnet ports will be σ_x = 44.2 μm and σ_y = 15.7 μm. This is almost a factor of two smaller vertical beam size than SOLEIL, and so the diffraction limited performance should be possible to extend to approximately λ = 400 nm, in the visible. Different focusing optics could extend this range even further towards the VUV.

Conclusions

We have presented careful measurements of the lateral spatial resolution at ALS Beamline 1.4.4 and have found they agree very well with the theoretical resolution given by the optical magnification and electron beam source size. A functional form of the beam size is used to fit the measured data, and is then used to show how the resolution performance will scale as a function of selected optics (numerical aperture of the microscope objective) and as a function of electron beam size for different example synchrotrons. Beamline designers can use these results to help balance throughput, spatial resolution and working distance requirements of their user programs. As accelerator beam sizes get smaller in newer machines, the diffraction-limited performance can be extended to frequencies above the infrared.

Acknowledgements

We would like to thank Fernando Sannibale for information on electron beam emittances and source sizes in synchrotron light sources. This work and the Advanced Light Source are supported by the Director, Office of Science, Office of Basic Energy Sciences, Materials Sciences Division, of the U.S. Department of Energy under Contract No. DE-AC02-05CH11231 at Lawrence Berkeley National Laboratory.

References

ALS Storage Ring Parameters, http://www.als.lbl.gov/als/techspecs/srparameters.html

Bertrand, L., Doucet, J., Dumas, P., Simionovici, A., Tsoucaris, G., Walter, P., (2003). *J. Synchrotron Radiation* **10**, 387–392.

Born, Max & Wolf, Emil, (1999). *Principles of Optics*, p. 371, Cambridge University Press.

Carr, G. L., J. A. Reffner, and G. P. Williams, (1995). *Rev. Sci. Instrum.* **66,** 1490.

Carr, G. L., (2001). *Rev. Sci. Instrum.* **72**, 1613.

Dumas, Paul & Tobin, Mark J., (2003). *Spectroscopy Europe* **15**, 17-23.

Hecht, E., (1998). *Optics*, p. 416, Addison Wesley Longman, Inc.

Hirschmugl, C.J., (1994). Ph.D. Thesis, Yale University.

Holman, Hoi-Ying N., Martin, Michael C., Blakely, Eleanor A., Bjornstad, Kathy, McKinney, Wayne R., (2000). *Biopolymers (Biospectroscopy)* **57**, 329-335

Holman, Hoi-Ying N., Martin, Michael C., McKinney, Wayne R., (2003). *Spectroscopy – An International Journal* **17**, 139-159.

Holman, Hoi-Ying N. & Martin, Michael C., (2006). *Advances in Agronomy* **90**, 79-127.

Keller, L.P., *et al.*, (2006). *Science* **314**, 1728-1731.

Kim, K.-J., (1989). "Characteristics of Synchrotron Radiation," in Physics of Particle Accelerators, AIP Conf. Proc. 184, Am. Inst. Phys., New York.

Levenson, Erika, Lerch, Philippe, Martin, Michael C., (2006). *Infrared Physics and Technology* **49**, 45-52.

Li, Z. Q., Wang, G. M., Sai, N., Moses, D., Martin, M. C., Di Ventra, M., Heeger, A. J., Basov, D. N., (2006). *Nano Letters* **6**, 224-228.

Martin, Michael C. & McKinney, Wayne R., (1998). *Proceed. Mater. Res. Soc.* **524**, 11.

Martin, Michael C. & McKinney, Wayne R., (2001). *Ferroelectrics* **249**, 1-10.

Miller, L.M., Smith, G.D., Carr, GL, (2003). *J. Biological Physics* **29**, 219-230.

Miller, L.M. & Dumas, P., (2006). *Biochim Biophys Acta.* **1758**, 846-57.

MIL-STD-150A, Section 5.1.1.7, *USAF 1951 3-Bar Resolving Power Target*; also see http://www.efg2.com/Lab/ImageProcessing/TestTargets/

Raab, T.K. & Martin, M.C., (2001). *Planta* **213**, 881-887.

Rayleigh, (1879). *Phil. Mag.* **8** (5), 261.

Reffner, J. A., P. A. Martoglio, and G. P. Williams, (1995). *Rev. Sci. Instrum.* **66,** 1298.

Russ, John C., (1986). *Practical Stereology*, p. 9, Plenum Press, New York, NY.

Russ, John C., (2002). *The Image Processing Handbook*, p. 320, CRC Press, Boca Raton, FL.

SOLEIL Parameters at the Source points, http://www.synchrotron-soleil.fr/portal/page/portal/SourceAccelerateur/ParametresPointsSources

Summary of NSLS-II Source Properties, http://www.bnl.gov/nsls2/project/source_properties.asp

Veiseh, Mandana, Veiseh, Omid, Martin, Michael C., Bertozzi, Carolyn, Zhang, Miqin, (2007). *Biosensors and Bioelectronics* **23**, 253-260.

VUV Storage Ring Parameters, (2006). http://www.nsls.bnl.gov/facility/accelerator/vuv/vuv_parameters.pdf

Figure Captions

Figure 1. Resolution test definitions. (a) The step edge resolution test fits a Gaussian function to the first derivative of the measured profile. Resolution is given by the full width at half maximum (FWHM) of the Gaussian. (b) The imaging resolution test uses Rayleigh's criterion to determine if the peaks are resolved. (c) A micrograph of the USAF 1951 3-Bar Resolving Test Chart. The blue line indicates where the line scan was preformed over the edge of the larger square for the step edge tests. The red box shows group 8 of the test chart where an imaging test example shown in (d) was obtained.

Figure 2. Step edge resolution test results as a function of wavelength. The FWHM resolution was measured with two detectors to cover the mid- and near-IR spectral ranges. A fit of the data to the effective source size discussed in the text is shown in red, with the two components of the fit, diffraction and electron beam source size, shown with dashed lines. Inset: Example raw data of step edge profiles.

Figure 3. Imaging resolution test results as a function of wavelength. A fit of the data to the effective source size discussed in the text is shown in red, with the two components of the fit, diffraction and electron beam source size, shown with dashed lines. Insets: Example profiles of the smallest bars at 1.11 μm (just resolved) and 1.43 μm (not resolved) and the corresponding Gaussian fits.

Figure 4. Upper panel: The predicted change in the resolution when using lower numerical aperture objectives. Lower panel: The predicted change in the resolution due to the different electron beam source sizes at different synchrotron light sources.

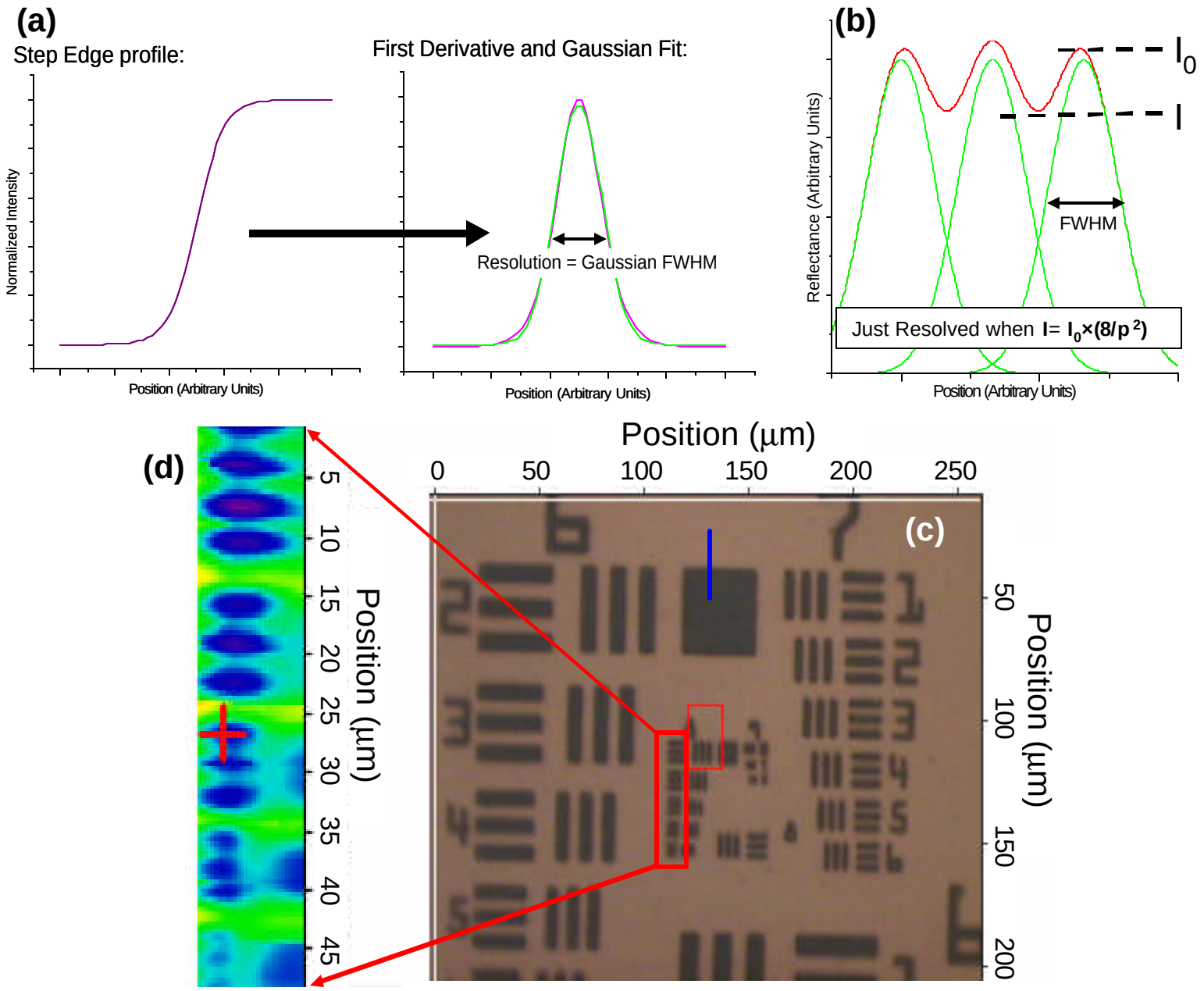
(a)
Step Edge profile:
First Derivative and Gaussian Fit:
Normalized Intensity
Position (Arbitrary Units)
Resolution = Gaussian FWHM
Position (Arbitrary Units)
(b)
I_0
I
Reflectance (Arbitrary Units)
FWHM
Just Resolved when $I = I_0 \times (8/p^2)$
Position (Arbitrary Units)
(d)
Position (μm)
0
50
100
150
200
250
(c)
5
10
15
20
25
30
35
40
45
Position (μm)
50
100
150
200
Position (μm)

Figure 1

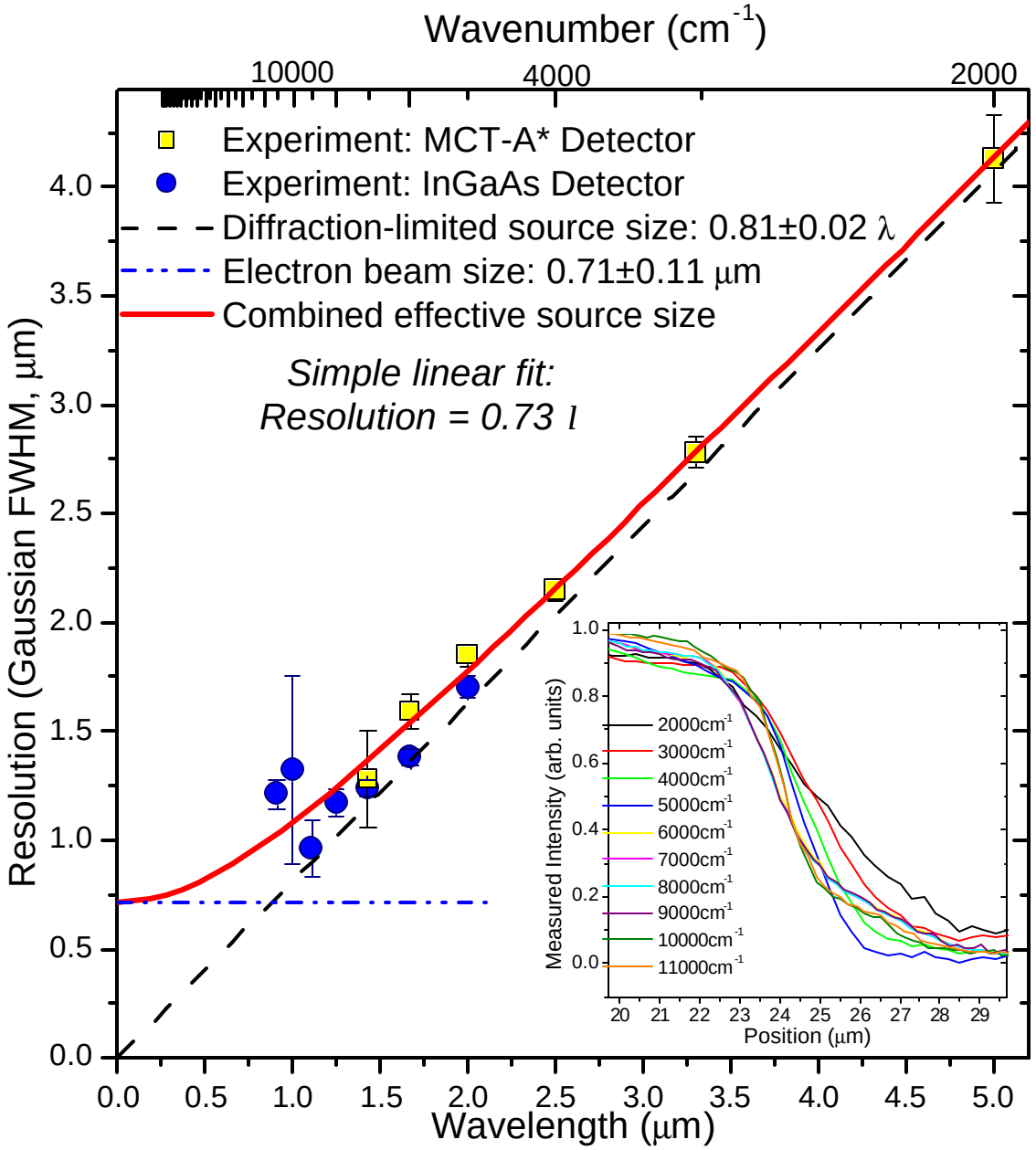
Wavenumber (cm-1)
10000
4000
2000
Experiment: MCT-A* Detector
Experiment: InGaAs Detector
Diffraction-limited source size: 0.81±0.02 λ
Electron beam size: 0.71±0.11 μm
Combined effective source size
Simple linear fit:
Resolution = 0.73 l
Resolution (Gaussian FWHM, μm)
Wavelength (μm)
0.0
0.5
1.0
1.5
2.0
2.5
3.0
3.5
4.0
4.5
5.0
Measured Intensity (arb. units)
Position (μm)
2000cm-1
3000cm-1
4000cm-1
5000cm-1
6000cm-1
7000cm-1
8000cm-1
9000cm-1
10000cm-1
11000cm-1

Figure 2

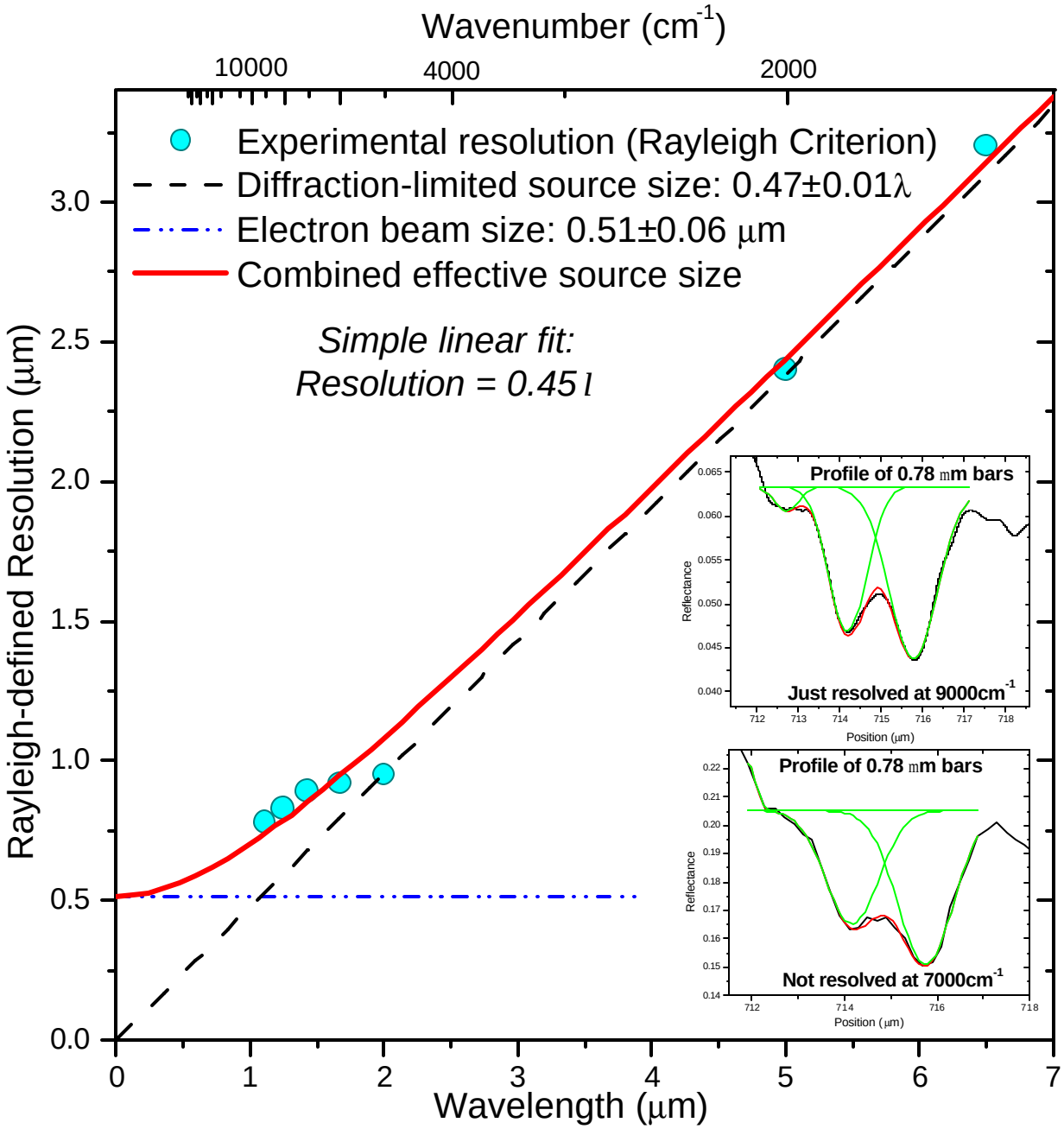
Wavenumber (cm-1)
10000
4000
2000
Experimental resolution (Rayleigh Criterion)
Diffraction-limited source size: 0.47±0.01λ
Electron beam size: 0.51±0.06 μm
Combined effective source size
Simple linear fit:
Resolution = 0.45λ
Rayleigh-defined Resolution (μm)
Wavelength (μm)
Profile of 0.78 mm bars
Just resolved at 9000cm-1
Reflectance
Position (μm)
Profile of 0.78 mm bars
Not resolved at 7000cm-1
Reflectance
Position (μm)

Figure 3

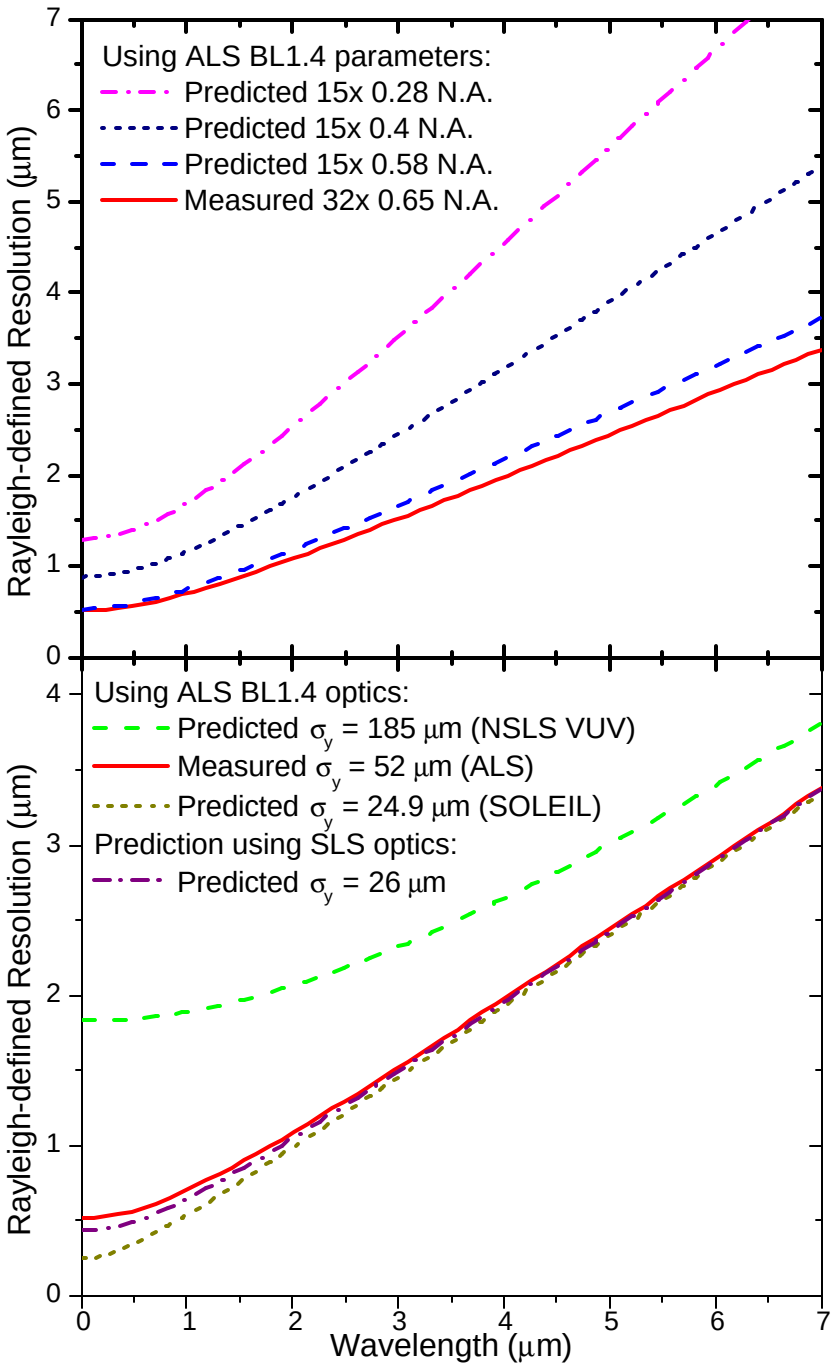
Using ALS BL1.4 parameters:
Predicted 15x 0.28 N.A.
Predicted 15x 0.4 N.A.
Predicted 15x 0.58 N.A.
Measured 32x 0.65 N.A.
Rayleigh-defined Resolution (μm)
Using ALS BL1.4 optics:
Predicted σy = 185 μm (NSLS VUV)
Measured σy = 52 μm (ALS)
Predicted σy = 24.9 μm (SOLEIL)
Prediction using SLS optics:
Predicted σy = 26 μm
Rayleigh-defined Resolution (μm)
Wavelength (μm)

Figure 4